

# Modulation properties of optically injection-locked quantum cascade lasers

Cheng Wang,<sup>1,2,\*</sup> Frédéric Grillot,<sup>2</sup> Vassilios I. Kovanis,<sup>3</sup> Joshua D. Bodyfelt,<sup>4</sup> and Jacky Even<sup>1</sup>

<sup>1</sup>Université Européenne de Bretagne, INSA, CNRS FOTON, 20 avenue des buttes de Coesmes, 35708 Rennes Cedex 7, France

<sup>2</sup>Telecom Paristech, Ecole Nationale Supérieure des Télécommunications, CNRS LTCI, 46 rue Barrault, Paris 75013, France

<sup>3</sup>Air Force Research Laboratory, 2241 Avionics Circle, Wright-Patterson AFB, Dayton, Ohio 45433, USA

<sup>4</sup>Electro Science Laboratory, Ohio State University, 1320 Kinnear Road, Columbus, Ohio 43212, USA

\*Corresponding author: cheng.wang@insa-rennes.fr

Received March 28, 2013; revised May 1, 2013; accepted May 3, 2013;

posted May 6, 2013 (Doc. ID 187971); published May 30, 2013

A rate equation analysis on the modulation response of an optical injection-locked quantum cascade laser is outlined. It is found that the bifurcation diagram exhibits both bistable and unstable locked regions. In addition, the stable locked regime widens as the linewidth enhancement factor increases. It is also shown that both positive and negative optical detunings as well as strong injection strength enhance the 3 dB modulation bandwidth by as much as 30 GHz. Finally, the peak in the modulation response is significantly influenced by the optical frequency detuning. © 2013 Optical Society of America

OCIS codes: (140.3518) Lasers, frequency modulated; (140.3520) Lasers, injection-locked; (140.5960) Semiconductor lasers; (140.5965) Semiconductor lasers, quantum cascade.

<http://dx.doi.org/10.1364/OL.38.001975>

The optical injection locking architecture has recently emerged as a powerful engine for establishing tunable photonic oscillators and high-bandwidth radio frequency links. For intersubband quantum cascade (QC) laser geometries, the suppression of residual amplitude modulation was observed [1], as well as power scaling, linewidth reduction, and frequency noise suppression of frequency combs [2]. Theoretically, the modulation bandwidth enhancement was presented via a simple model without taking into account gain stage cascading [3–5], while the stability map describing bifurcations of an optically injected QC laser has been analytically examined in [5]. This Letter aims to theoretically investigate the bifurcation diagram as well as the intensity modulation (IM) properties of injection-locked single mode QC lasers through a full-rate equation model, especially the role of optical detuning in enhancing the modulation bandwidth within the associated response.

Following the carrier dynamics of a single mode QC laser described in [6], as well as the complex field of an injection-locked laser reported in [7], the rate equations for optical injection-locked QC lasers are given by

$$\frac{dN_3}{dt} = \eta \frac{I}{q} - \frac{N_3}{\tau_{32}} - \frac{N_3}{\tau_{31}} - G_0 \Delta N S, \quad (1)$$

$$\frac{dN_2}{dt} = \frac{N_3}{\tau_{32}} - \frac{N_2}{\tau_{21}} + G_0 \Delta N S, \quad (2)$$

$$\frac{dN_1}{dt} = \frac{N_3}{\tau_{31}} + \frac{N_2}{\tau_{21}} - \frac{N_1}{\tau_{out}}, \quad (3)$$

$$\frac{dS}{dt} = (N_{pd} G_0 \Delta N - 1/\tau_p) S + \beta N_{pd} \frac{N_3}{\tau_{sp}} + 2k_c \sqrt{S_{inj}} S \cos \Delta \phi, \quad (4)$$

$$\frac{d\Delta\phi}{dt} = \frac{\alpha_H}{2} (N_{pd} G_0 \Delta N - 1/\tau_p) - \Delta\omega_{inj} - k_c \sqrt{\frac{S_{inj}}{S}} \sin \Delta\phi, \quad (5)$$

where  $N_{3,2,1}$  respectively denote the carrier numbers in the upper subband, lower subband, and bottom state.  $S$  denotes the active photon number, and the phase difference is  $\Delta\phi = \phi_{slave} - \phi_{master}$  where  $\phi_{master}$ ,  $\phi_{slave}$  are the phases of the master and slave lasers, respectively. The frequency detuning is  $\Delta\omega_{inj} = \omega_{master} - \omega_{slave}$  where  $\omega_{master}$  is the angular frequency of the master laser and  $\omega_{slave}$  that of the slave laser, while  $k_c$  denotes the coupling rate of the master into the slave. The relaxation times are  $\tau_{32}$ ,  $\tau_{31}$ ,  $\tau_{21}$ ,  $\tau_{out}$  is the tunneling out time,  $\tau_p$  is the photon lifetime and  $\tau_{sp}$  is the spontaneous emission time. The gain stage number is  $N_{pd}$ , while  $\Delta N = N_3 - N_2$  is the population inversion, and  $G_0$  is the gain coefficient. The linewidth enhancement factor (LEF) is  $\alpha_H$ . The injection ratio is defined as  $R_{inj} = S_{inj}/S_{FE}$ , where  $S_{inj}$  is the injected photon number and  $S_{FE}$  is the photon number of the free running case. All parameters used in our computations are outlined in [6].

The bifurcation diagrams are useful to identify nonlinear dynamics, such as period doubling and large four-wave mixing regions in optically injected semiconductor lasers [8]. In this work, we investigate the main saddle-node (SN) and Hopf bifurcations using the continuation package “Matcont” [9]. Our computations are summarized in Fig. 1. The stable locking regime is bounded by the supercritical bifurcations, which is enlarged by increasing the LEF from 0 to 2.5. In contrast to the case of interband lasers, zero detuning of QC lasers is always stable even under low injection level. Besides, the codimension-two SN-Hopf points are of Bogdanov–Takens (BT) form instead of zero-Hopf form [10], where the bifurcations change criticality. Note that complex nonlinear dynamics appear around the codimension-two points [8]. With a larger LEF, BT<sub>1</sub> moves toward the negative axis of injection ratio associated with the positive axis of detuning,

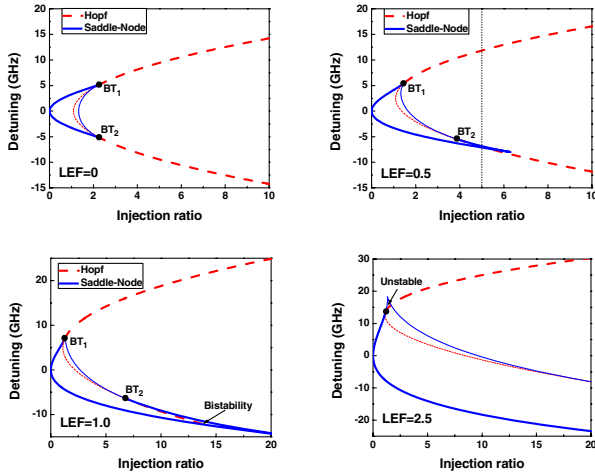


Fig. 1. Local bifurcation diagram of an injection-locked QC laser for LEF values of 0, 0.5, 1.0, and 2.5. Solid line is the saddle-node (SN) bifurcation and dashed line is the Hopf bifurcation. The supercritical bifurcation is denoted by thick lines while subcritical bifurcation by thin lines. The stable locking regime is bounded by the supercritical bifurcations. The investigated laser is operating in the stable locked region of the bifurcation diagram with an LEF of 0.5, where the vertical dotted line indicates an injection ratio of 5.0.

while  $BT_2$  moves oppositely. For  $LEF = 0$  the bifurcation is symmetric, while nonzero LEF leads to an asymmetric bifurcation diagram. A bistability region emerges near the cusp point at the negative detuning side for  $LEF = 1.0$ , which is not exhibited in conventional interband semiconductor lasers [11]. For  $LEF = 2.5$ , a small unstable locked area appears at the positive detuning side. When compared to interband lasers, all above differences in the bifurcation diagram can be directly attributed to the high ratio of the photon lifetime to the carrier lifetime in QC lasers ( $\tau_p/\tau_{32} = 1.85$ ) [11]. In addition, the simulation shows that a large LEF increases the peak amplitude in the modulation response.

With the bifurcation diagram, the modulation properties of the injection-locked QC laser can be studied in the stable locked regime. To investigate the IM response, we linearize the rate equations via the standard approach of small signal analysis. The modulation transfer function is

$$H(\omega) = \frac{p_1 p_2 p_3 p_4 p_5}{z_1 z_2 z_3} \frac{\prod_{k=1}^3 (j\omega - z_k)}{\prod_{k=1}^5 (j\omega - p_k)}, \quad (6)$$

where  $z_k, p_k$  are respectively the zeros and poles of the steady-state polynomials, which are useful in the modulation response's behavior analysis with respect to the Bode plots. Among the zeros,  $z_1$  is the smallest and is expressed as

$$z_1 = k_c \sqrt{S_{inj}/S} (\cos \phi - \alpha_H \sin \phi). \quad (7)$$

It is known that the free running QC lasers exhibit a rather flat IM response without a resonance peak due to their ultrafast carrier lifetime [12]. The modulation bandwidth can be enhanced by increasing the bias current; however, this is limited by the excess heating and the degradation of spectral properties. The inset of Fig. 2

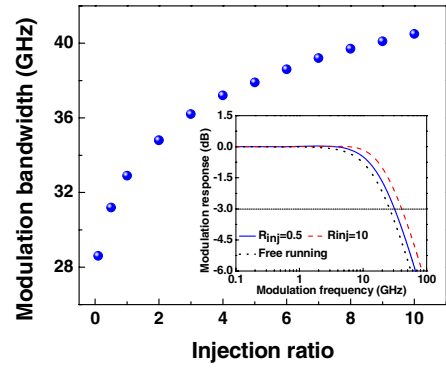


Fig. 2. Main: 3 dB modulation bandwidth as a function of the injection ratio (for zero detuning and  $LEF = 0.5$ ). Inset: related IM response. Note the absence of any peaks.

illustrates that the injection-locked laser at zero detuning does not present a resonance peak as well. Figure 2 also shows that the 3 dB modulation bandwidth increases with the optical injection strength; however, the bandwidth tends to saturate at even higher injection ratios. The possible underlying physical mechanism to this saturation is the finite carrier and photon lifetimes, which remain open for further investigation in the future.

In Fig. 3 we present the detuning effect on the modulation response. The detuning range is controlled in the stable locked regime with respect to the bifurcation diagram. It is seen that the 3 dB bandwidth is enhanced by both positive and negative detunings, while the former is more efficient. From the inset, under both detunings it is found that peaks arise in the response. However, from Bode plot analysis, the underlying mechanisms are different. For the positive detuning, a pair of complex conjugate poles appear that indicates a resonance originating from the interaction between the locked field and the shifted cavity-resonance field. In such a way, the resonance frequency is given by [13]:

$$\omega_R = \Delta\omega_{inj} - \frac{\alpha_H}{2} (N_{pd} G_0 \Delta N - 1/\tau_p). \quad (8)$$

The resonance combined with the small zero  $z_1$  results in the peak. In the case of negative detuning, all the poles are real and the peak is due to the fact that the zero  $z_1$  is

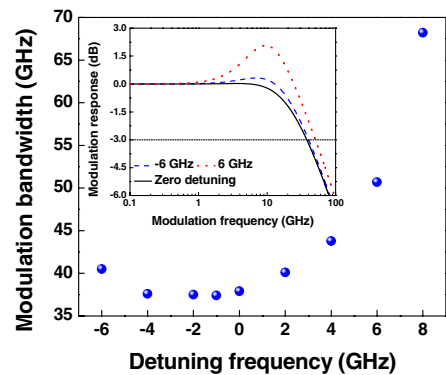


Fig. 3. Main: 3 dB modulation bandwidth as a function of detuning (for  $R_{inj} = 5.0$  and  $LEF = 0.5$ ). Inset: IM response under various detuning conditions. Note the appearance of the resonance peak under positive detuning.

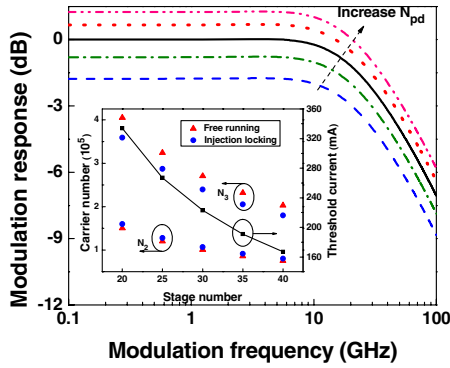


Fig. 4. IM response for various gain stage numbers increasing from 20 to 40, note that it is normalized to the case with  $N_{pd} = 30$  (under zero detuning and  $R_{inj} = 5.0$ ). Inset is steady-state result for  $I_{bias} = 1.5I_{th}$ . Photon population for the free running laser is  $S_{FE} \approx 7.2 \times 10^6$ , and for the injection-locked laser  $S \approx 13.3 \times 10^6$ .

smaller than any of the poles. However, we note that since there is no resonance under negative detuning for QC lasers, Eq. (8) derived from interband lasers requires further confirmation.

One fundamental feature of QC lasers is the multistage cascade scheme, where electrons contribute to the gain and the photon emission in each period, leading to a quantum efficiency proportional to the period number [14]. We therefore study the influences of the cascade gain stage number on the IM response. Surprisingly, it is shown that the response is slightly impacted by the stage number, both in free running and injection-locked lasers under the same bias-threshold current ratio ( $I_{bias} = 1.5I_{th}$ ). However, when all the responses are normalized to the DC value  $H(0)$  with  $N_{pd} = 30$ , as shown in Fig. 4, it is found that the amplitude of the response increases with a larger stage number, which means more power is obtained in the modulation, while the response shape remains similar. In contrast, the inset of Fig. 4 presents that the steady-state property is strongly impacted by the stage number. With more gain stages in the QC laser, both carriers in the upper and lower subbands decrease, while the photon number remains almost constant. Additionally, the threshold current of the free running laser is substantially reduced, while the differential efficiency ( $dS/dI$ ) is enhanced, as reported in [14]. When compared to the free running laser, the carrier number of the upper subband ( $N_3$ ) in the locked laser decreases while that of the lower subband ( $N_2$ ) slightly increases. The population in the bottom state remains constant at  $N_1 = \tau_{out}\eta I/q$ . Besides, the laser power is scaled up. On the other hand, laser devices with more stages require higher operating voltage, which is useful to reduce the undesired potential drops in the injector region, but it also leads to poor heat-removal efficiency from the active region [15].

In conclusion, we presented a theoretical analysis of optical injection-locked QC lasers, both on bifurcation

maps and modulation responses. It was demonstrated that the stable locking regime widens as the LEF value increases. Meanwhile, both the bistable and the unstable locked regions are found in this dynamical system. In addition, a large LEF increases the peak amplitude in the IM response. Increasing either the injection ratio or the master-slave frequency difference enhances the 3 dB modulation bandwidth. The cascade gain stage number mainly influences the steady-state properties, such as the decrease of the current threshold and carrier populations with more gain stages. These findings are of prime importance for the performance enhancement of QC lasers, suggesting that an optical injection-locked experiment is now needed for further investigations.

Dr. Frédéric Grillot's work is supported by the European Office of Aerospace Research and Development (EOARD) under grant number FA8655-12-1-2093. Dr. Vassilios Kovanis is supported via the AFOSR Electromagnetics Portfolio of Dr. Arje Nachman. Cheng Wang's work is supported by China Scholarship Council. The authors would like to thank C. Otto from Technische Universität Berlin, Germany; Prof. Thomas Erneux of Université Libre de Bruxelles, Dr. S. Barbieri and Prof. Carlo Sirtori of Université Paris Diderot-Paris 7, France for helpful discussion; and J. L. Volaris for a stimulating research environment at OSU-ESL.

## References

1. M. S. Taubman, T. L. Myers, B. D. Cannon, and R. M. Williams, *Spectrochimica Acta Part A* **60**, 3457 (2004).
2. S. Borri, I. Galli, F. Cappelli, A. Bismuto, S. Bartalini, P. Cancio, G. Giusfredi, D. Mazzotti, J. Faist, and P. De Natale, *Opt. Lett.* **37**, 1011 (2012).
3. B. Meng and Q. J. Wang, *Opt. Express* **20**, 1450 (2012).
4. C. Wang, F. Grillot, V. Kovanis, and J. Even, *J. Appl. Phys.* **113**, 063104 (2013).
5. T. Erneux, V. Kovanis, and A. Gavrielides, "Stability boundaries of injected quantum cascade lasers," *Phys. Rev. E*, submitted for publication.
6. Y. Petitjean, F. Destic, J. C. Mollier, and C. Sirtori, *IEEE J. Sel. Top. Quantum Electron.* **17**, 22 (2011).
7. R. Lang, *IEEE J. Quantum Electron.* **18**, 976 (1982).
8. S. Wiczorek, B. Krauskopf, T. B. Simpson, and D. Lenstra, *Phys. Rep.* **416**, 1 (2005).
9. A. Dhooge, W. Govaerts, and Y. A. Kuznetsov, *ACM TOMS* **29**, 141 (2003).
10. J. Pausch, C. Otto, E. Tylaite, N. Majer, E. Scholl, and K. Ludge, *New J. Phys.* **14**, 053018 (2012).
11. B. Kelleher, S. P. Hegarty, and G. Huyet, *Phys. Rev. E* **86**, 066206 (2012).
12. W. Maineult, L. Ding, P. Gellie, P. Filloux, and C. Sirtori, *Appl. Phys. Lett.* **96**, 021108 (2010).
13. A. Murakami, K. Kawashima, and K. Atsuki, *IEEE J. Quantum Electron.* **39**, 1196 (2003).
14. J. Faist, A. Tredicucci, F. Capasso, C. Sirtori, D. L. Sivco, J. N. Baillargeon, A. L. Hutchinson, and A. Y. Cho, *IEEE J. Quantum Electron.* **34**, 336 (1998).
15. E. Tournié and A. N. Baranov, *Semicond. Semimet.* **86**, 183 (2012).